ARTICLE OPEN

Check for updates

NRF2 signaling plays an essential role in cancer progression through the NRF2-GPX2-NOTCH3 axis in head and neck squamous cell carcinoma

Xiaoye Jin[1,2], Xiayuan Lou[1,2], Haoxiang Qi[3], Chao Zheng[1,2], Bo Li[1,2], Xuerong Siwu[1,2], Ren Liu[1,2], Qiaoli Lv[4], An Zhao[5], Jian Ruan[6] and Ming Jiang[1,2]✉

The activation of nuclear factor erythroid 2–related factor 2 (NRF2) has been observed in various cancers. Yet its exact contribution to the development of head and neck squamous cell carcinoma (HNSCC) remains undetermined. We previously found that NRF2 signaling is critical for the differentiation of squamous basal progenitor cells, while disruption of NRF2 causes basal cell hyperplasia. In this study, we revealed a correlation between elevated NRF2 activity and poor outcomes in HNSCC patients. We demonstrated that NRF2 facilitates tumor proliferation, migration, and invasion, as evidenced by both in vitro and in vivo studies. Significantly, NRF2 augments the expression of the antioxidant enzyme GPX2, thereby enhancing the proliferative, migratory, and invasive properties of HNSCC cells. Activation of GPX2 is critical for sustaining cancer stem cells (CSCs) by up-regulating NOTCH3, a key driver of cancer progression. These results elucidate that NRF2 regulates HNSCC progression through the NRF2-GPX2-NOTCH3 axis. Our findings proposed that pharmacological targeting of the NRF2-GPX2-NOTCH3 axis could be a potential therapeutic approach against HNSCC.

Oncogenesis (2024)13:35 ; https://doi.org/10.1038/s41389-024-00536-z

INTRODUCTION

Head and neck squamous cell carcinoma (HNSCC) represents a diverse group of cancers arising from the squamous cells lining the mucosal surfaces of the head and neck region, including the oral cavity, oropharynx, larynx, and hypopharynx [1]. HNSCC is one of the most common cancers worldwide, accounting for over 870,000 cases per year [2]. Tobacco use, alcohol consumption, and human papillomavirus (HPV) infection are the primary etiological factors [3]. Genetic alterations are common in HNSCC including growth factor receptors (e.g., EGFR), tumor suppressors (e.g., p53) and signaling pathways (e.g., PI3K), etc [4–6]. Despite advances in surgical techniques, radiation therapy, and chemotherapy, the overall survival rates for HNSCC have only modestly improved over the past few decades. The development of resistance to therapy, the presence of distant metastases at diagnosis, and the significant morbidity associated with treatment highlight the need for innovative therapeutic strategies. Recent advancements in immunotherapy and targeted therapies offer new hope for improving outcomes in HNSCC patients. However, the cure rate for advanced HNSCC patients remains poor and only 40–50% of patients survive for 5 years [7].

NRF2 signaling is pivotal in maintaining cellular redox homeostasis and defending against oxidative stress. NRF2 operates as a master regulator, controlling the expression of various genes involved in antioxidant response and detoxification processes to maintain cellular redox homeostasis. The regulation of NRF2 expression is intricately controlled through its interaction with KEAP1 to form a CUL3-based E3 ubiquitin ligase complex. This KEAP1-mediated ubiquitination and subsequent proteasomal degradation of NRF2 ensures that NRF2 levels remain low under unstressed conditions [8, 9]. Upon oxidative stress, modifications in KEAP1 lead to the stabilization and nuclear translocation of NRF2, where it binds to antioxidant response elements (ARE) in the DNA to activate the transcription of its target genes. Multiple studies have shown that NRF2 plays a paradoxical role in cancer development. Activation of NRF2 in normal cells promotes antioxidant defenses and detoxification, protecting against DNA damage and mutagenesis, thus acting as a tumor suppressor by eliminating potential cancer initiation [10, 11]. However, the constitutive activation of NRF2 in cancer cells enhances cancer cell proliferation, metabolic reprogramming, and resistance to chemotherapy and radiotherapy, thus promoting tumor progression and metastasis [12–16]. Clinical evidence also indicates that elevated expression of NRF2 is significantly associated with poor prognosis [16, 17]. This duality highlights the complexity of NRF2 signaling in the cancer milieu.

[1]Center for Genetic Medicine, the Fourth Affiliated Hospital, Zhejiang University School of Medicine, Hangzhou, China. [2]Institute of Genetics, Zhejiang University International School of Medicine, Zhejiang Provincial Key Laboratory of Genetic & Developmental Disorders, Hangzhou, China. [3]School of Pharmacy and Department of Hepatology, the Affiliated Hospital of Hangzhou Normal University, Hangzhou Normal University, Hangzhou, China. [4]Institute of Cancer Research, Jiangxi Cancer Hospital, Nanchang, China. [5]Institute of Cancer Research, Zhejiang Cancer Hospital, Hangzhou, China. [6]Department of Medical Oncology, The First Affiliated Hospital, School of Medicine, Zhejiang University and Key Laboratory of Cancer Prevention and Intervention, Ministry of Education, Hangzhou, China. ✉email: mj2735@zju.edu.cn

Received: 5 April 2024 Revised: 13 September 2024 Accepted: 18 September 2024
Published online: 27 September 2024

Glutathione peroxidases (GPXs) are selenium-containing enzymes crucial in the defense of oxidative stress by reducing peroxides with the oxidization of glutathione (GSH) to glutathione disulfide (GSSG) [18, 19]. There are eight GPX family members who have distinct cellular locations and substrate specificities, contributing to various physiological functions beyond their antioxidant roles [20]. GPX members play multifaceted roles in cancers as both tumor-suppressive and oncogenic activities depending on the context and specific family member involved [21–23]. GPX4 has been identified as a critical player in conferring resistance to ferroptosis, garnering attention as a potential novel target for anticancer therapies [24]. GPX7 has been demonstrated to be downregulated and hypermethylated in gastric cancer, and its reconstitution suppresses tumor cell growth [25]. GPX8 has been implicated in the promotion of cancer cell growth [26]. Recent studies have shown that GPX2 serves as a predictive marker for recurrence-free survival in prostate cancer and promotes cancer development through the Wnt/β-catenin/EMT pathway [27]. Previous studies also indicate that the expression level of GPX2 is a prognostic factor in esophageal squamous cell carcinoma (ESCC), correlating with clinicopathological features [28]. In addition, Kazi et al. suggests that GPX2 as a targetable factor influences immune escape in cold tumors, thus affecting the response to immune checkpoint inhibitors [29].

In this study, we observed that GPX2 was significantly overexpressed in patients with *NRF2* mutations in HNSCC, contributing to accelerated tumor progression compared to patients with normal *NRF2*. We further found that NRF2 enhances GPX2 expression, influencing the NOTCH pathway by sustaining NOTCH3 levels. Reduction of GPX2 level led to a decrease in tumor cell growth both in vitro and in vivo. Moreover, increased levels of GPX2 were observed in HNSCC patients, correlating with poorer patient outcomes. This study sheds light on the critical role of the NRF2-GPX2-NOTCH3 axis in advancing HNSCC, suggesting that targeting the NRF2-GPX2-NOTCH3 axis might offer a novel strategy to enhance treatment efficacy in HNSCC.

RESULTS

Enhanced NRF2 signaling correlates with poor survival rates in patients with HNSCC

The NRF2 degradation complex is crucial in the regulation of NRF2 signaling and comprises KEAP1 and CUL3 components. To investigate the role of NRF2 components in HNSCC, we performed an extensive analysis utilizing The Cancer Genome Atlas (TCGA) database. About 12% of all cancers carried mutations in at least one of these three genes (Fig. 1A). *NRF2* mutations are present in about 6% of HNSCC cases (Fig. 1A), consistent with previous report [30]. In addition, we analyzed the occurrence of mutations in *KEAP1* and *CUL3*, and identified at rates of 4% and 2%, respectively (Fig. 1A). Notably, the missense mutations of *NRF2* in the Neh 2 domain primarily impaired its capacity to bind to KEAP1, enhancing its nuclear translocation and prolonging its activity (Fig. 1A, B). Mutations of *KEAP1* were found not only in the DGR (Kelch) domain, which is crucial for NRF2 interaction, but also in various structural domains, and a similar pattern is observed in *CUL3* as well (Supplementary Fig. 1). Following stress stimuli, the activation of NRF2 promotes a broad spectrum of downstream target genes involved in various cellular processes such as iron catabolism (*FTH1*, *FTL*), metabolism (*G6PD*, *TKT*), antioxidant signaling (*TXN*, *GCLC*, *GCLM*), and xenobiotic transformation (*NQO1*) [31]. Increased expression of these genes was observed in patients harboring *NRF2* mutations (Fig. 1C). Subsequent analysis suggested that upregulation of NRF2 downstream genes correlated with decreased overall survival rate in patients (Fig. 1D and Supplementary Fig. 2) [32]. Notably, high expression of NRF2 markedly enhanced cell proliferation compared to cells with lower levels of NRF2, as evidenced by Ki67 staining (Fig. 1E). Furthermore, the expression levels of KEAP1 increased with the activation of NRF2, which may be due to a reciprocal feedback mechanism (Fig. 1C, E). The results indicate that missense mutations in *NRF2* are associated with poor prognoses in patients with HNSCC.

NRF2 is essential for HNSCC progression in vitro and in vivo

Multiple studies have demonstrated that the activation of NRF2 acts protectively against tumor initiation [11, 33, 34]. In contrast, sustained activation of NRF2 is associated with the progression of various cancers, substantially enhancing resistance to cancer treatments [35–37]. To elucidate the role of NRF2 in the progression of HNSCC, the *NRF2* gene was specifically knocked out in the FaDu cell line using CRISPR-Cas9 technology. This knockout was confirmed by reduced expression of *NRF2* target genes, *NQO1* and *GCLC* (Fig. 2A, B). Deletion of *NRF2* resulted in a notable decline in cell proliferation, demonstrated by decreased cell growth rates and colony formation capabilities (Fig. 2C, D). Deletion of *NRF2* also led to a significant reduction in both the size and number of spheres formed (Fig. 2E). We further found that deletion of *NRF2* markedly impaired the ability of migration and invasion (Fig. 2F). In addition, deletion of *NRF2* significantly increased the cellular level of reactive oxygen species (ROS) determined by DCFH-DA flow cytometry (Fig. 2G and Supplementary Fig. 3). There was a significant increase in apoptotic cells in *NRF2*-deleted cells compared to control cells (Fig. 2H). Furthermore, following injection into nude mice (2×10^6 cells per injection), tumors initiated by *NRF2*-deleted cells were observably smaller compared to those derived from control cells (Fig. 2I). Immunohistochemistry (IHC) staining revealed that the deletion of *NRF2* significantly reduced Ki67 staining intensity (Fig. 2J). Suppressing *NRF2* by shRNA knockdown in Detroit 562 cells significantly reduced proliferation, migration, and invasion capabilities, consistent with those observed in FaDu cells (Supplementary Fig. 4).

GPX2 is a potential downstream target of NRF2 signaling

To elucidate the role of NRF2 in the progression of HNSCC, we performed RNA sequencing analysis in both control and *NRF2* knockout FaDu cells. Gene expression profiling, as well as the associated biological processes and pathways, were evaluated. We identified a list of differentially expressed genes. 707 genes (~66.95%) were upregulated, and 349 genes (~33.05%) were down-regulated following *NRF2* knockout (Fig. 3A). By targeting differentially expressed mRNAs, the Kyoto Encyclopedia of Genes and Genomes (KEGG) pathway enrichment analysis revealed that the differentially expressed mRNAs were predominantly associated with cellular processes and metabolism (Fig. 3B). Heatmap cluster analysis of metabolic-related genes revealed that the gene expression profiles between the control and *NRF2* knockout cells were distinct (Fig. 3C). Correspondingly, these gene expression differences were also represented in the volcano plot (Fig. 3D). Among these genes, the mRNA expression of *GPX2* was notably suppressed in the *NRF2* knockout cells (Fig. 3C, D). RT-qPCR and WB confirmed that the expression of *GPX2* was decreased in FaDu and Detroit 562 cells after deletion of *NRF2* (Fig. 3E and Supplemental Fig. 4A). In cohort study of TCGA database, the mRNA expression levels of *GPX2* were positively correlated with *NRF2* in both normal tissues and tumor tissues (Fig. 3F). Simultaneously, we observed a significant upregulation of *GPX2* expression in tumor tissues with *NRF2* mutations compared to normal tissues. Conversely, the low expression of *GPX2* in tumor tissues without *NRF2* mutations is attributed to their low *NRF2* expression levels (Fig. 3G). The K-M analysis showed that high levels of *GPX2* were associated with a poor survival ratio in HNSCC patients (Fig. 3H).

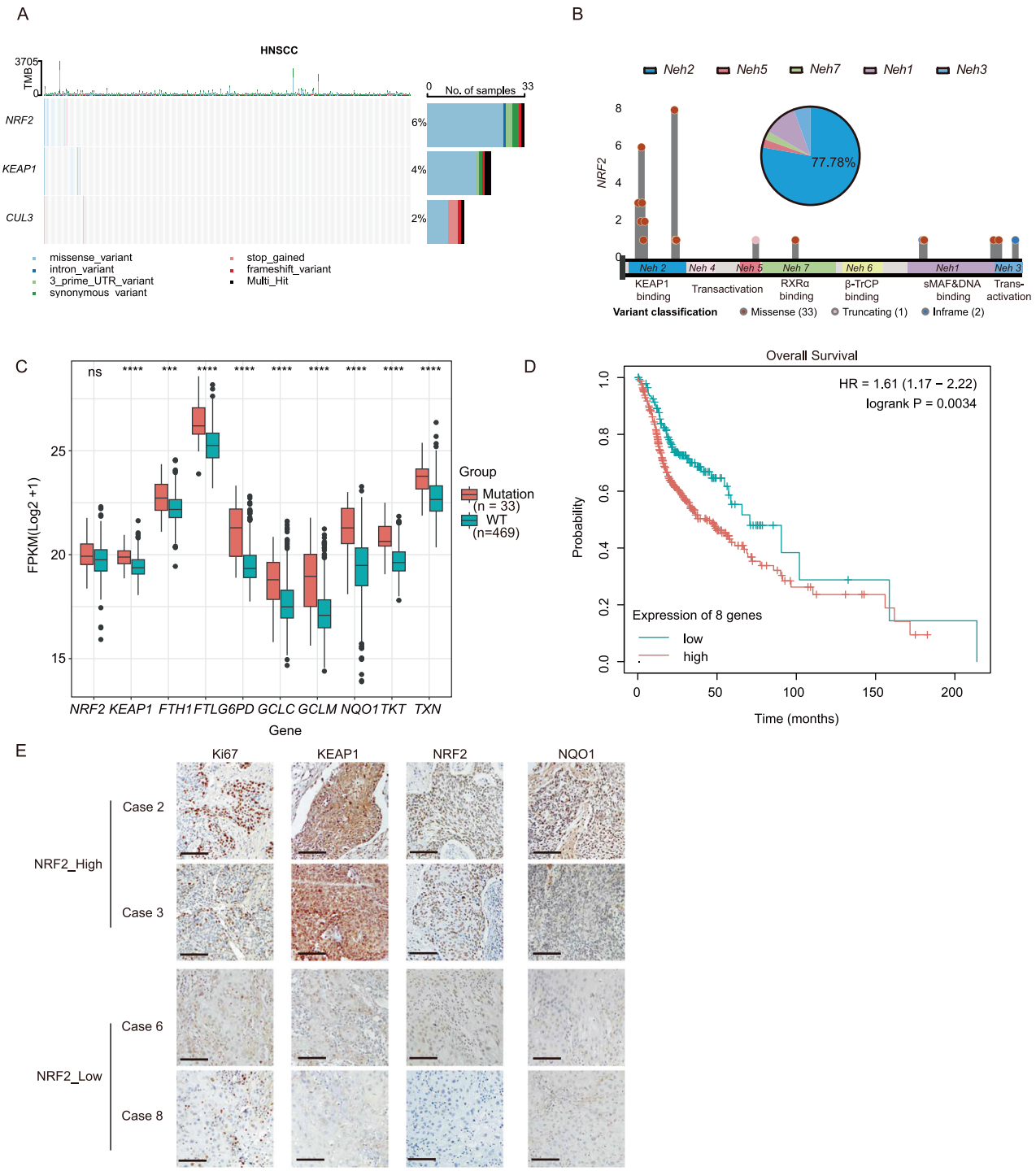

Fig. 1 NRF2 was correlated with poor prognosis. A The oncoplot showed the mutation frequency of *NRF2*, *KEAP1*, and *CUL3* genes. **B** Lollipop plot showed somatic alterations of the *NRF2* gene in the TCGA-HNSCC cohort. The pie chart displayed the proportion of mutations in each domain. **C** Increased expression levels of *KEAP1*, *FTH1*, *FTL*, *GCLC*, *GCLM*, *G6PD*, *NQO1*, *TKT*, and *TXN* were observed in patients with *NRF2* mutations in the TCGA-HNSCC cohort ($n = 502$). Mean ± SD, ***$P < 0.001$, ****$P < 0.0001$, ns, no significant. **D** K-M analysis showed that high expression levels of *NRF2*-regulated genes were correlated with a poor prognosis in HNSCC in the TCGA-HNSCC cohort ($n = 499$). **E** Representative immunohistochemical staining demonstrated that cells with high NRF2 expression exhibited markedly enhanced cell proliferation measured by Ki67 staining in HNSCC patients (scale bar = 100 μm). FPKM Fragments Per Kilobase of exon model per Million mapped fragments.

GPX2 promotes tumor growth in HNSCC

To explore the role of GPX2 in the malignant processes of HNSCC, we performed lentivirus-mediated shRNA knockdown of *GPX2* in FaDu and Detroit 562 cell lines. The knockdown efficiency was confirmed by RT-qPCR and western blot (Fig. 4A, B and Supplementary Fig. 5A). Inhibition of GPX2 caused a significant reduction in cell proliferation measured by growth rate and colony formation assay (Fig. 4C, D and Supplementary Fig. 5B). *GPX2* knockdown reduced the size of the tumor spheres formed in the 3D culture system (Fig. 4E). FaDu and Detroit 562 cells exhibited

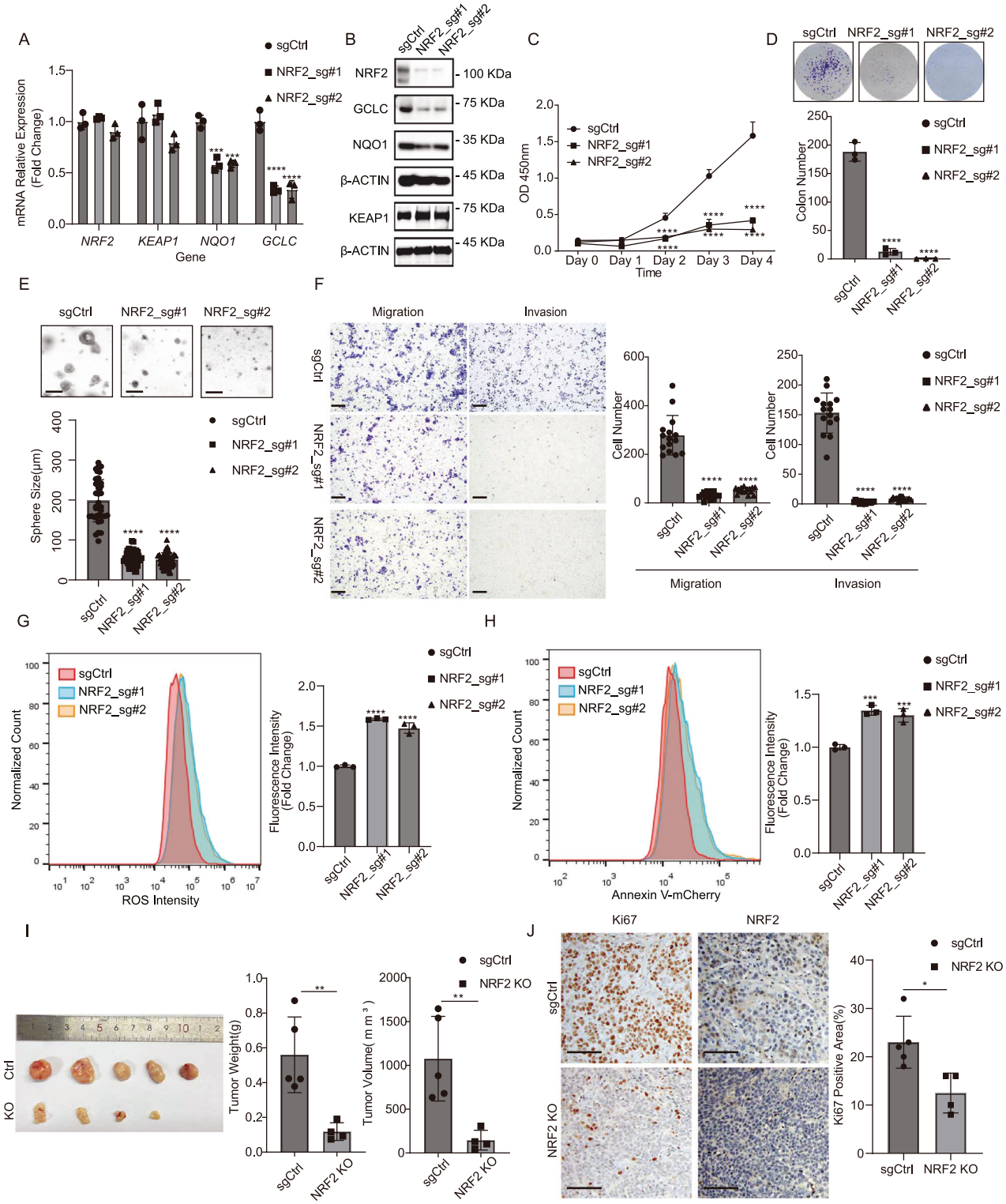

Fig. 2 NRF2 promoted tumor growth in vitro and in vivo. A The mRNA expression levels of *NQO1* and *GCLC* in FaDu cells were reduced upon *NRF2* knockout measured by RT-qPCR analysis. Mean ± SD, $n = 3$. $^{****}P < 0.0001$. **B** The protein levels of NRF2, GCLC, and NQO1 in FaDu cells were reduced following NRF2 depletion. **C** Proliferation of FaDu cells was significantly inhibited upon *NRF2* knockout. Mean ± SD, $n = 3$, $^{****}P < 0.0001$. **D** Colony formation capability of FaDu cells was impaired upon *NRF2* knockout. Mean ± SD, $n = 3$, $^{****}P < 0.0001$. **E** The ability of FaDu cells to form spheres was impaired upon *NRF2* knockout (scale bar =200μm). Mean ± SD, $n > 3$, $^{****}P < 0.0001$. **F** The abilities of migration and invasion in FaDu cells were impaired upon *NRF2* knockout (scale bar = 200 μm). Mean ± SD, $n = 3$, $^{****}P < 0.0001$. **G** NRF2 depletion dramatically induced ROS levels in FaDu cells measured by flow cytometry. Mean ± SD, $n = 3$, $^{****}P < 0.0001$. **H** NRF2 depletion dramatically induced apoptosis in FaDu cells assessed by Annexin V-mCherry staining. Mean ± SD, $n = 3$, $^{***}P < 0.001$. **I** NRF2 depletion significantly suppressed subcutaneous tumor growth in nude mice ($n = 5$ for each group). Mean ± SD, $^{**}P < 0.01$. **J** Representative immunohistochemical staining demonstrated that NRF2 depletion markedly suppressed cell proliferation measured by Ki67 staining (scale bar = 100 μm). Mean ± SD, $n = 5$, $^{*}P < 0.05$.

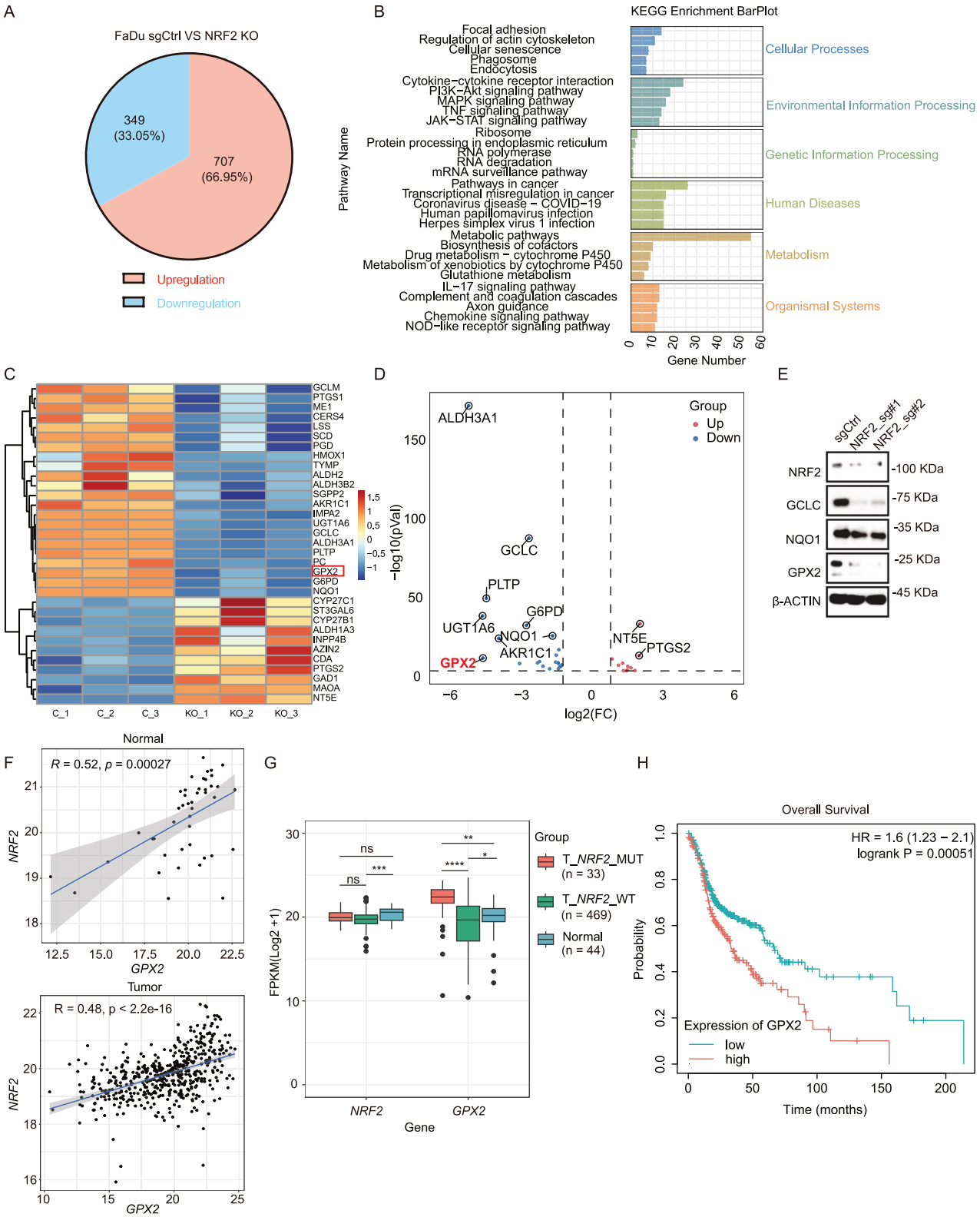

Fig. 3 GPX2 was a potential downstream target of NRF2 signaling. A RNA-Seq identified 707 upregulated and 349 downregulated genes following NRF2 depletion in FaDu cells. **B** Gene categories were significantly enriched ($P \leq 0.05$) for genes with altered expression in KEGG pathways in FaDu cells upon *NRF2* knockout. **C** A heatmap displays the changes in expression of various metabolic genes in FaDu cells upon *NRF2* knockout. **D** Volcano plot showed the differential expression of genes (DEGs) following NRF2 depletion. Blue, downregulated genes; Red, upregulated genes. **E** Reduced protein levels of GCLC, NQO1, and GPX2 were observed in FaDu cells following NRF2 depletion. **F** The mRNA expression levels of *GPX2* were positively correlated with *NRF2* expression in both normal and tumor tissues ($R = 0.52$, $p = 00027$ vs $R = 0.48$, $p < 2.2e\text{-}16$). **G** Increased expression levels of *GPX2* were observed in patients with *NRF2* mutations in the TCGA-HNSCC cohort ($n = 546$). Mean ± SD,****$P < 0.0001$. **H** K-M analysis showed that high expression levels of *GPX2* were correlated with a poor prognosis in HNSCC from the TCGA-HNSCC cohort ($n = 499$).

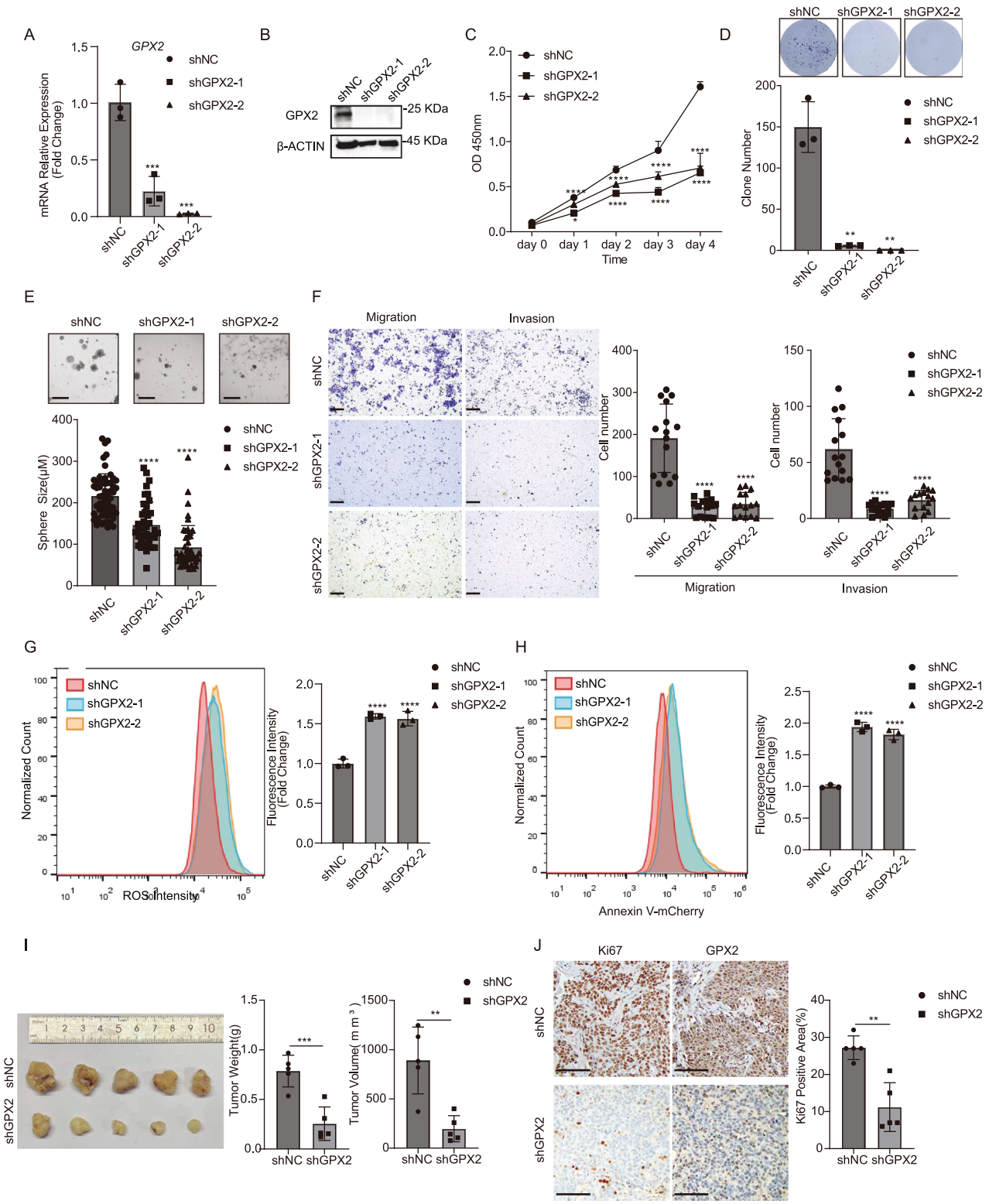

Fig. 4 GPX2 promoted tumor growth in vitro and in vivo. A *GPX2* expression in FaDu cells was reduced upon *GPX2* knockdown measured by RT-qPCR analysis. Mean ± SD, $n = 3$, $^{***}P < 0.001$. **B** The protein levels of GPX2 in FaDu cells were reduced following NRF2 depletion. **C** Proliferation of FaDu cells was significantly inhibited upon *GPX2* knockdown. Mean ± SD, $n = 3$, $^{*}P < 0.05$, $^{****}P < 0.001$. **D** Colony formation capability of FaDu cells was impaired upon *GPX2* knockdown. Mean ± SD, $n = 3$, $^{**}P < 0.01$. **E** The ability of FaDu cells to form spheres was impaired upon *GPX2* knockdown (scale bar = 200 μm). Mean ± SD, $n > 3$, $^{****}P < 0.0001$. **F** The abilities of migration and invasion in FaDu cells were impaired upon *GPX2* knockdown (scale bar = 200 μm). Mean ± SD, $n = 3$, $^{****}P < 0.0001$. **G** GPX2 depletion dramatically induced ROS levels in FaDu cells measured by flow cytometry. Mean ± SD, $n = 3$, $^{****}P < 0.0001$. **H** GPX2 depletion dramatically induced apoptosis in FaDu cells assessed by Annexin V-mCherry staining. Mean ± SD, $n = 3$, $^{***}P < 0.001$. **I** GPX2 depletion significantly suppressed subcutaneous tumor growth in nude mice ($n = 5$ for each group). Mean ± SD, $^{***}P < 0.001$. **J** Representative immunohistochemical staining demonstrated that GPX2 depletion markedly suppressed cell proliferation measured by Ki67 staining (scale bar = 100 μm). Mean ± SD, $n = 5$, $^{**}P < 0.01$.

decreased migrating and invasive capability following *GPX2* knockdown (Fig. 4F and Supplementary Fig. 5C). Meanwhile, *GPX2* knockdown significantly increased the cellular level of ROS (Fig. 4G and Supplementary Fig. 5D). An increase in the proportion of apoptotic cells was also observed in *GPX2* knockdown cells (Fig. 4H and Supplementary Fig. 5E). Moreover, *GPX2* knockdown in FaDu cells led to smaller xenograft tumors and reduced proliferation than in controls (Fig. 4I, J).

Depletion of GPX2 Expression disrupts NOTCH3 expression

NRF2 signaling is activated in cancer stem cells (CSCs) and contributes to CSC properties, such as proliferation, metastasis, and therapeutic resistance [13, 38]. Meanwhile, GPX2 can maintain the genomic integrity of pluripotent stem cells through antioxidant defense [39–41]. GPX2 is concentrated in stem cells and proliferative compartments of epithelial tissues to maintain tissue integrity and homeostasis [20]. To test whether *GPX2* is involved in the maintenance of CSCs, we analyzed the proportion of CSCs in FaDu cells by flow cytometry analysis, using CD44 and ALDH activity, the common markers for CSCs [42, 43]. Loss *of NRF2 or GPX2* markedly diminished the proportion of CSCs (Fig. 5A, B and Supplementary Figs. 6 and 7). We examined the expression levels of 17 genes that encode multidrug-resistant proteins(MRPs) for cancer stem cells and identified 4 genes (*ABCC1*, *ABCC3*, *ABCC5,* and *ABCC10*) with relatively high expression for further analysis [44]. Our result revealed that the deletion of NRF2 led to a reduction in the expression of *ABCC1*, *ABCC3*, and *ABCC5*, aligning with the previous findings that *ABCC1* is significantly downregulated in glioblastoma cells following *NRF2* knockout (Supplementary Fig. 8A, B) [45]. In contrast, the knockdown of *GPX2* did not affect the expression of chemoresistance proteins but slightly increased the expression of *ABCC1* (Supplementary Fig. 8C). Wnt, Hedgehog (HH), and NOTCH are canonical CSC pathways crucial to the tumorigenicity of CSCs [46]. We found that depletion of *GPX2* significantly reduces HH and NOTCH signaling (Supplementary Fig. 9A, C). We further found that the NOTCH target gene, *HES1*, is highly expressed in HNSCC cells. In contrast, the expression levels of *GLI1* and *GLI2* are either low or undetectable (Supplementary Fig. 9B). To determine the specific NOTCH signaling implicated downstream of GPX2, we first examined all NOTCH ligands and receptors in the TCGA database. We revealed that the high mRNA expression levels of *NOTCH2* and *NOTCH3* are positively correlated with *GPX2* (Supplementary Fig. 10). We further detected that *GPX2* predominantly regulates the expression of *NOTCH3* in HNSCC cells (Fig. 5C, D and Supplementary Fig. 9D). According to RNA-seq data from the FaDu cell line, we found a significant decrease of *NOTCH3* following *NRF2* knockout (Fig. 5C, D and Supplementary Fig. 11). The cohort analysis of the TCGA database demonstrated a strong association between the mRNA expression of *NOTCH3* and *GPX2* ($R = 0.33$, $p = 6.1e\text{-}15$; Fig. 5E, F and Supplementary Fig. 12).

NOTCH3 is critical for HNSCC progression

To determine whether activation of NOTCH3 is responsible for promoting the CSC phenotype of HNSCC, we performed lentivirus-mediated shRNA knockdown of *NOTCH3* in FaDu cells. The knockdown efficiency was confirmed by RT-qPCR and western blot (Fig. 6A, B). Inhibition of NOTCH3 caused a significant reduction in cell proliferation, as measured by growth rate and colony formation assay (Fig. 6C, D). *NOTCH3* knockdown reduced the size of the tumor spheres formed in the 3D culture system (Fig. 6E). Additionally, FaDu cells exhibited decreased migrating and invasive capability following *NOTCH3* knockdown (Fig. 6F). *NOTCH3* knockdown significantly increased the cellular level of ROS (Fig. 6G). An increase in the proportion of apoptotic cells was also observed in *NOTCH3* knockdown cells (Fig. 6H). The depletion of *NOTCH3* markedly diminished the proportion of CSCs (Fig. 6I and Supplementary Fig. 13). Moreover, *NOTCH3* knockdown in FaDu cells led to smaller xenograft tumors and reduced proliferation than in controls (Fig. 6J). Consistently, high expression of GPX2 markedly enhanced NOTCH3 levels in HNSCC patients (Fig. 6K). Therefore, these results suggest that NOTCH signaling, mediated by NOTCH3, promotes the progression of HNSCC.

DISCUSSION

The role of NRF2 in the malignant progression of cancers has emerged as a focal point of contemporary oncological research. Notably, activation of NRF2 has been associated with a poorer overall survival rate in various cancers, suggesting that NRF2 may play a critical role in cancer pathogenesis [47]. Yet the molecular mechanisms of NRF2 regulating cancer progression remain unexplored. In this study, we elucidated that GPX2 functions as a downstream target of NRF2 in HNSCC. The patients exhibiting elevated activation of NRF2 experience an upregulation of *GPX2* mRNA, correlating with decreased overall survival rates. We demonstrate that GPX2 regulates HNSCC cell proliferation, migration, and metastasis by regulating CSC phenotype. Analysis of TCGA database revealed that mRNA expression of *NOTCH3* was significantly higher in patients with increased *GPX2* expression. We further revealed that the inhibition of GPX2 notably reduced the expression of NOTCH3 in both FaDu and Detroit 562 cells. These findings suggest a pivotal role for the NRF2-GPX2-NOTCH3 axis in NOTCH3-mediated regulation of CSCs in HNSCC (Fig. 7).

NRF2 mutations are specifically frequent in multiple squamous cell carcinomas (SCC) of the lung, skin, esophagus, and larynx [30, 48, 49]. Most of these SCC-associated *NRF2* mutations harbor gain-of-function activity [50]. Our analysis of a cohort of HNSCC cases has elucidated the clinical relevance of *NRF2* mutation. We identified that approximately 12% of patients exhibited mutations in the NRF2 complex. These mutations were strongly correlated with tumor progression and emerged as a significant prognostic factor.

Numerous studies have highlighted that activation of *NRF2* contributes to cancer progression and metastasis, while also endowing resistance to chemotherapy and radiotherapy [12–16]. Our study suggests that NRF2 regulates the expression of multidrug-resistant proteins ABCC1, ABCC3, and ABCC5, potentially contributing to the chemoresistance observed in cancer cells with activated NRF2. Recent studies have revealed that NRF2 directly regulates the expression of gene groups that are related to cellular metabolism, in addition to the detoxification response [51]. Upon depleting NRF2, we revealed that the most significantly altered genes were predominantly linked to cellular metabolism. We further found that GPX2 was significantly reduced in *NRF2* knockout cells.

GPX2 is glutathione peroxidase, playing a crucial role in maintaining cellular redox balance by regulating the levels of reactive oxygen and nitrogen species. It functions within the antioxidant system, leveraging the GSH (reduced glutathione) and GSSG (oxidized glutathione) cycle to protect cells against oxidative damage [52]. The antioxidant function of GPX2 is evident not only by its enzymatic activity but also by its upregulation in response to oxidative stress. A prominent pathway for the induction of GPX2 expression involves the KEAP1/NRF2 complex [53]. Kleeburger's group further identified potential NRF2 activation sites within the *GPX2* gene, suggesting a direct regulatory mechanism by NRF2 on GPX2 expression [54]. An increasing number of studies indicate that GPX2 is also involved in the development of cancers [27, 28]. Many studies have shown that high level of GPX2 promotes tumor growth, metastasis, and drug resistance, while reducing its expression helps inhibit tumor development [27, 55]. When we depleted GPX2 in HNSCC, the growth of tumor cells was significantly inhibited, while the proportion of apoptotic cells

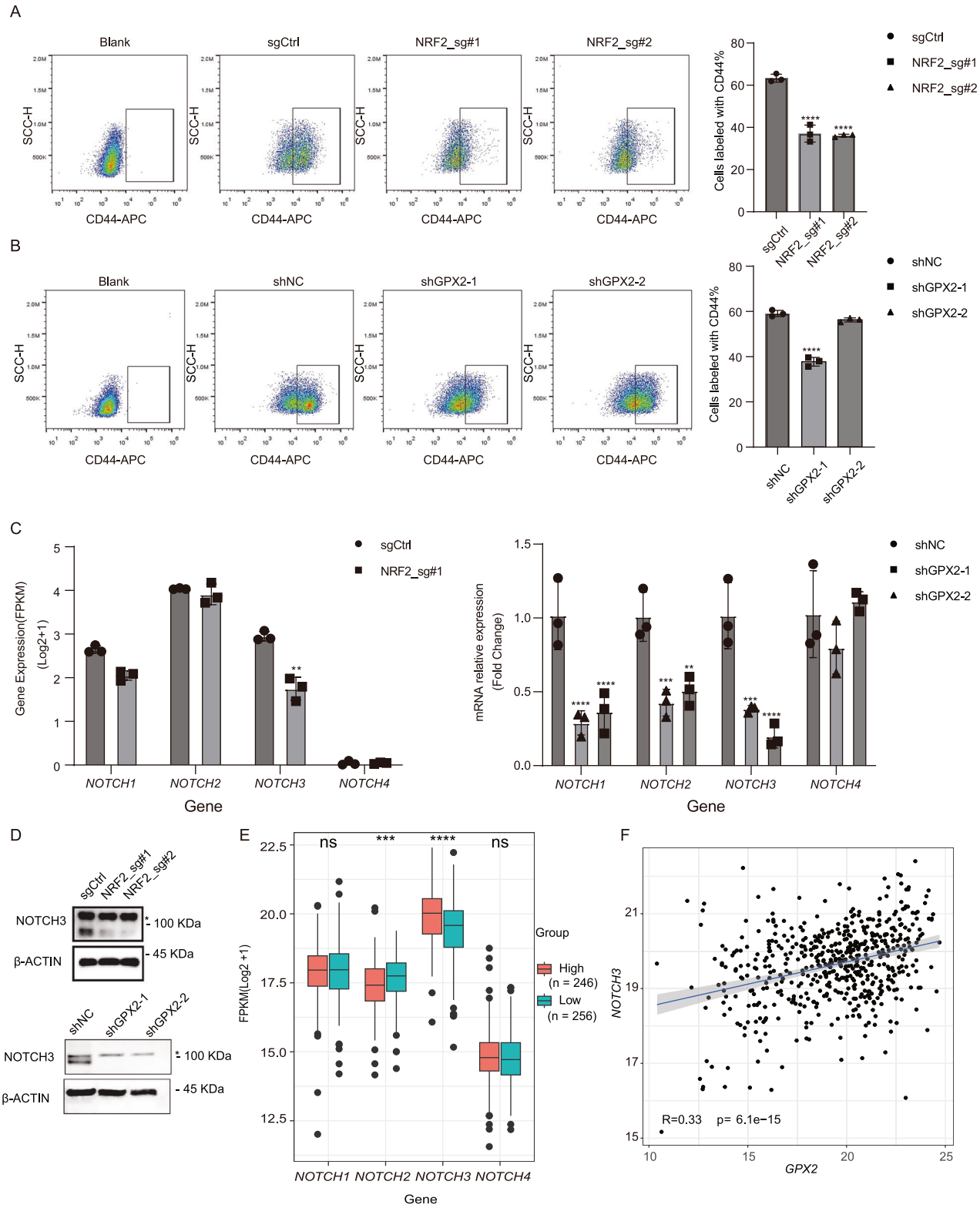

Fig. 5 *GPX2* expression was correlated with *NOTCH3* expression level in HNSCC. A The proportion of CSCs in FaDu cells was markedly diminished upon *NRF2* knockout by CD44 staining. Mean ± SD, $n = 3$, $^{****}P < 0.0001$. **B** The proportion of CSCs in FaDu cells was markedly diminished upon *GPX2* knockdown by CD44 staining. Mean ± SD, $n = 3$, $^{****}P < 0.0001$. **C** *NOTCH3* expression in FaDu cells was significantly reduced upon *NRF2* knockout by RNA-Seq. Additionally, the mRNA expression levels of *NOTCH1*, *NOTCH2*, and *NOTCH3* in FaDu cells were reduced by RT-qPCR analysis. Mean ± SD, $n = 3$, $^{**}P < 0.01$, $^{***}P < 0.001$, $^{****}P < 0.0001$. **D** The protein levels of NOTCH3 in FaDu cells were reduced following the depletion of either NRF2 or GPX2. "*" is an unspecific band. **E** Increased expression levels of *NOTCH3* were observed in patients with high *GPX2* expression in the TCGA-HNSCC cohort ($n = 502$). Mean ± SD, $^{**}P < 0.01$, $^{****}P < 0.0001$, ns no significant. **F** The mRNA expression levels of *NOTCH3* were positively correlated with *GPX2* expression ($R = 0.33$, $p = 6.1\text{e-}15$). Abbreviations: FPKM Fragments Per Kilobase of exon model per Million mapped fragments.

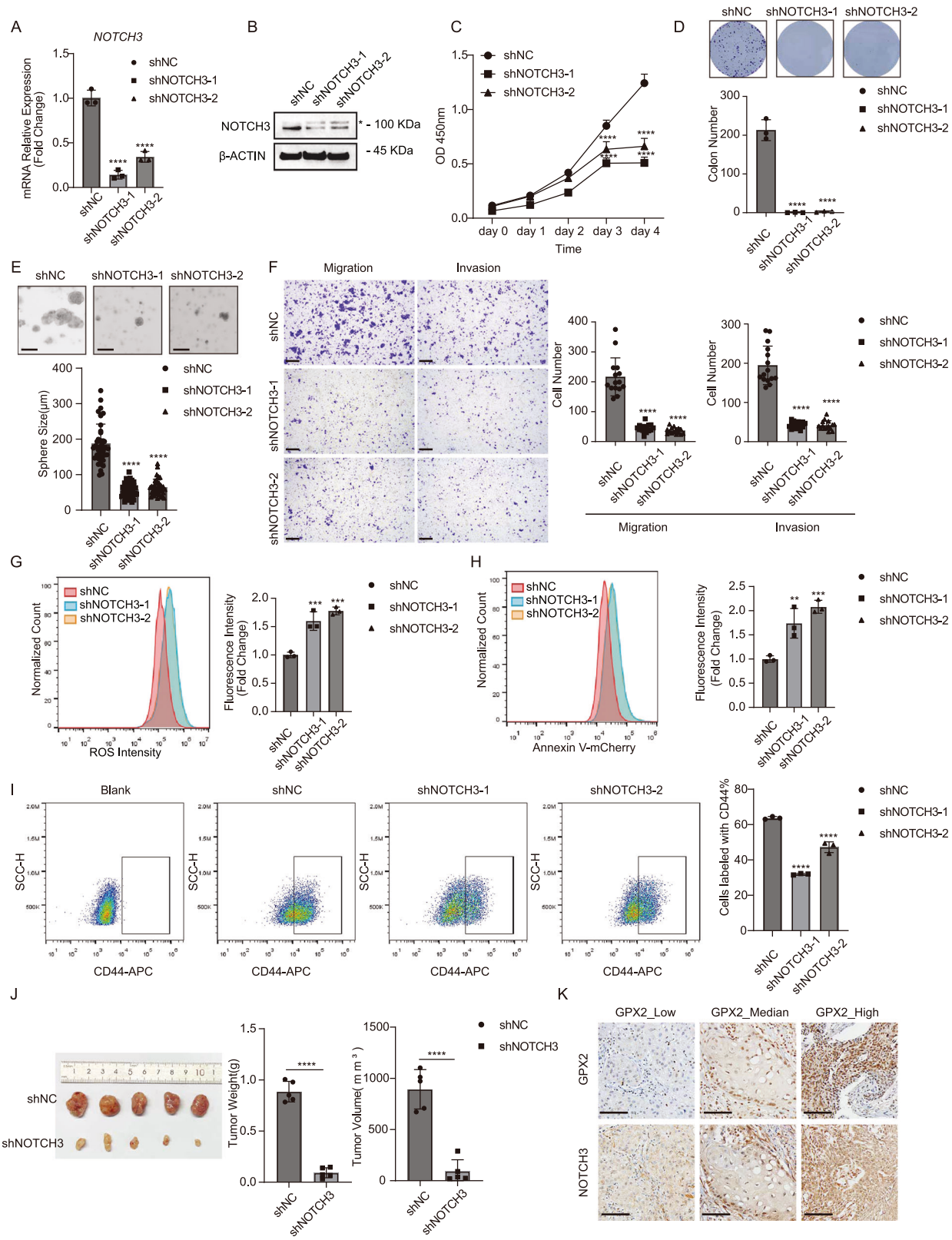

substantially increased. Indeed, GPX2 was demonstrated to play contrasting roles across various cancers. Inhibiting glutathione peroxidase (GPx) enzymes have been shown to enhance drug sensitivity [56, 57]. Elevated expression of the GPX2 is associated with chemoresistance in non-small cell lung cancers (NSCLCs) [58]. However, the knockdown of *GPX2* does not affect the expression of chemoresistance proteins in HNSCC cancer cells. MRPs play key roles in facilitating GSH export and maintaining its homeostasis, as well as exporting oxidized glutathione derivatives(e.g., glutathione disulfide (GSSG), S-nitrosoglutathione (GS-NO), and glutathione-

Fig. 6 *NOTCH3* regulated by *GPX2* promoted tumor growth in vitro and in vivo. A *NOTCH3* expression in FaDu cells was reduced upon *NOTCH3* knockdown measured by RT-qPCR analysis. Mean ± SD, $n = 3$, ****$P < 0.0001$. **B** The protein levels of NOTCH3 in FaDu cells were reduced following NOTCH3 depletion. "*" is an unspecific band. **C** Proliferation of FaDu cells was significantly inhibited upon *NOTCH3* knockdown. Mean ± SD, $n = 3$, ****$P < 0.0001$. **D** Colony formation capability of FaDu cells was impaired upon *NOTCH3* knockdown. Mean ± SD, $n = 3$, ****$P < 0.0001$. **E** The ability of FaDu cells to form spheres was impaired upon *NOTCH3* knockdown (scale bar = 200 μm). Mean ± SD, $n > 3$, ****$P < 0.0001$. **F** The abilities of migration and invasion in FaDu cells were impaired upon *NOTCH3* knockdown (scale bar = 200 μm). Mean ± SD, $n = 3$, ****$P < 0.0001$. **G** NOTCH3 depletion dramatically induced ROS levels in FaDu cells measured by flow cytometry. Mean ± SD, $n = 3$, ***$P < 0.001$. **H** NOTCH3 depletion dramatically induced apoptosis in FaDu cells assessed by Annexin V-mCherry staining. Mean ± SD, $n = 3$, **$P < 0.01$, ***$P < 0.0001$. **I** The proportion of CSCs in FaDu cells was markedly diminished upon *NOTCH3* knockdown by CD44 staining. Mean ± SD, $n = 3$, ****$P < 0.0001$. **J** NOTCH3 depletion significantly suppressed subcutaneous tumor growth in nude mice ($n = 5$ for each group). Mean ± SD, ****$P < 0.0001$. **K** Representative immunohistochemical staining demonstrated that GPX2 expression was strongly correlated with NOTCH3 in human HNSCC patients (scale bar = 100 μm).

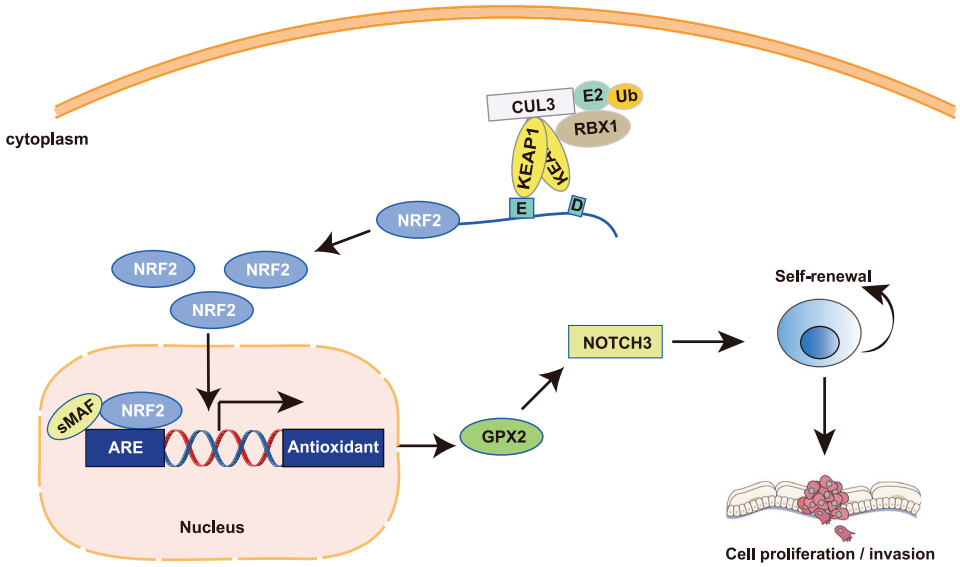

Fig. 7 A schematic diagram indicates the proposed mechanism of the NRF2-GPX2-NOTCH3 axis regulation in HNSCC progression.

metal complexes) and other GSH S-conjugates [59]. Depletion of GPX2 disrupts the intracellular GSH/GSSG ratio, leading to an excess of GSH within the cells. This imbalance may explain why GPX2 inhibition does not reduce the expression of chemoresistance genes. Concurrently, MRPs mediate the export of GSH, its oxidized derivatives, and GSH S-conjugates, which are crucial for maintaining cellular homeostasis and potentially contribute to drug resistance. Loss of GPX2 reduces oxidative phosphorylation (OXPHOS) and enhances aerobic glycolysis to promote malignant progression in breast cancer [23]. This controversial function of GPX2 could be attributed to tissue-specific factors.

We observed increased apoptosis caused by the absence of GPX2 in HNSCC. Considering a susceptibility of stem cells to apoptotic stimuli [41, 60], the emerging evidence following GPX2 depletion prompts us to test whether GPX2 promotes tumor progression by affecting CSCs. By performing CD44 staining and ALDEFLUOR assay on *GPX2* knockdown cells, we observed a significant reduction in the CSC population, indicating that *GPX2* plays a role in the maintenance of CSCs. Aberrant activation of pathways regulating stem cell self-renewal, such as NOTCH, Hedgehog (HH), and Wnt, are also pivotal in the tumorigenic potential of CSCs [46]. Dysregulation of these pathways contributes to tumor progression [61]. We examined all three signaling pathways and found that NOTCH signaling was disrupted in GPX2-depleted HNSCC cells, especially NOTCH3. The NOTCH signaling has been reported to associate with CSCs [62]. NOTCH1 and NOTCH2 facilitate cancer metastasis and contribute to a poor prognosis [63–65]. NOTCH3 promotes tumor development in various cancers, although it has been shown to inhibit tumor growth in breast cancer through the activation of PTEN and subsequent inhibition of the AKT-mTOR pathway [66]. Kondratyev M et al. have also verified the oncogenic role of NOTCH3 in HNSCC [67]. Of note, NRF2 is a direct activator of the *NOTCH3* enhancer, and the co-expression of NRF2 and NOTCH3 is associated with a poor prognosis in lung adenocarcinoma [68]. We further showed that loss of NOTCH3 dramatically reduced CSC population, subsequently preventing tumor growth and metastasis.

In conclusion, our findings illustrate that aberrant activation of NRF2 contributes to acquisition of malignant features and poor prognosis through NRF2-GPX2-NOTCH3 axis. Therefore, targeting the involvement of NRF2-GPX2-NOTCH3 axis holds potential as a therapeutic strategy for treating HNSCC characterized by NRF2 activation.

MATERIALS AND METHODS

Bioinformatic data collection and analysis

The transcriptome data and clinical information data of HNSCC patients were downloaded from UCSC XENA (https://xenabrowser.net/). Patients were divided into two groups based on the expression level of the corresponding genes. Volcano plot and boxplot were performed with R "ggplot2" package. The survival analysis was analyzed using the Kaplan-Meier plotter database (https://kmplot.com).

Tissue samples

Paraffin-embedded surgical tissue samples were collected from 5 patients with head and neck squamous cell carcinoma (HNSCC) who underwent curative surgery at Jiangxi Cancer Hospital (Jiangxi, China). The research was carried out in compliance with relevant national ethical guidelines and was approved by the Research Ethics Committee of Jiangxi Cancer Hospital under approval number (2024ky008).

Xenograft model

The animal experiments conducted in this study were ethically approved by the Institutional Animal Care and Use Committee of Zhejiang University (approval number: 20221576). Female and male Nu/Nu nude mice, aged six weeks, sourced from Slac (Shanghai, China), were utilized for the experiments. A total of 2×10^6 cells were subcutaneously injected into the nude mice in a random manner. Tumor volumes were calculated using the formula: $1/2 \times \text{length} \times \text{width}^2$. The mice were euthanized ~30–36 days post-injection, and the tumors were subsequently collected for further analysis.

Cell culture

FaDu and Detroit 562 cell lines were purchased from Procell Life Science &Technology (Wuhan, China). Cells were maintained in Dulbecco's Modified Eagle Medium (Gbico, MA, USA) supplemented with 10% fetal bovine serum (HATAKA, USA) and 1% penicillin-streptomycin (HATAKA) at 37 °C in a 5% CO_2 atmosphere. Cells were verified through short tandem repeat (STR) analysis and routinely screened for mycoplasma contamination.

Generation of *NRF2*^{KO}, *NRF2*^{KD}, *GPX2*^{KD}, *NOTCH3*^{KD} cell lines

NRF2^{KO} cells were established using pLentiCRISPRv2 expressing CAS9 and sgRNA described previously [69]. *NRF2*^{KD}, *GPX2*^{KD}, and *NOTCH3*^{KD} cell lines were established using lentiviral infection. Lentiviral vectors containing short hairpin RNAs targeting *NRF2*, *GPX2*, and *NOTCH3* were packaged into recombinant lentivirus using Lipofectamine™ 3000 (Thermofisher, MA, USA) in Opti-MEM medium according to the manufacturer's protocol. The target sequence for sh*NRF2*-1 is 5′- CTTGCATTAATTCGGGATATA-3′, for sh*NRF2*-2 is 5′- CCGGCATTTCACTAAACACAA -3′. The target sequence for sh*GPX2*-1 is 5′- GAAGGTAGATTTCAATACGTT-3′, for sh*GPX2*-2 is 5′- CCTACCCTTATGATGACCCAT-3′. The target sequence for sh*NOTCH3*-1 is 5′- GGTGATCGGCTCGGTAGTAAT-3′, for sh*NOTCH3*-2 is 5′- CCAATGCCAACT GAAGAGGAT-3′.

Colony formation assay

Cells were resuspended and cultured in 6-well plates (1000 cells/ well) in medium with 10% FBS containing 5% CO_2 about for 2 weeks. Cells were washed with PBS, fixed with 4% paraformaldehyde for 15 min and subsequently stained with 1% crystal violet (Biosharp, Beijing, China) for 10 min, subsequently imaged and quantified using ImageJ.

Cell growth assay

Cell growth was assessed through the utilization of the Cell Counting Kit-8 (CCK-8) (Vazyme, Nanjing, China). Cells were seeded at a density of 1500 cells per well into 96-well plates. 10 µl Cell Counting Kit-8 was added into each well. Then cells were incubated at 37 °C with 5% CO_2 for 2 h. The absorbance was measured at 450 nm by a microplate reader (BioTeK, Winooski, USA) at different time points.

Transwell assay

For the invasion assay, 24-well plates, containing 6.5 mm upper transwell chamber with 8 µm polycarbonate membranes (Corning, NY, USA) suspended over the wells, were coated with 15 µl of ice-cold Matrigel™ (Corning, NY, USA). A total of 1×10^5 cells was seeded into the upper chambers in 300 µl DMEM medium. A 500 µl volume of DMEM medium supplemented with 10% FBS was added to the lower chamber. Following a 48-h incubation, the cells located on the lower side of the membrane were fixed in 4% paraformaldehyde at room temperature for 20 min, stained with 1% crystal violet for 10 min, subsequently imaged and quantified using ImageJ. For the migration assay, a procedure similar to invasion assay was performed using the migration chamber without Matrigel and 5×10^4 cells were seeded.

Immunohistochemistry

The sections were deparaffinized and sequentially hydrated with xylene and gradient alcohol, respectively. They were further repaired with a citrate buffer, using 3% hydrogen peroxide to quench endogenous peroxidase activity, and then were blocked with BSA. Subsequently, the sections were incubated with primary antibodies (mouse anti-Ki67, BD Pharmingen, 610968, 1:1000; mouse anti-NRF2, Santa Cruz, 365949, 1:50; rabbit anti-GPX2, GeneTex, GTX100292, 1:1000; rabbit anti-NOTCH3, Abcam, ab23426, 1:1000; mouse anti-NQO1, Proteintech, 67240-1-Ig, 1:10000; rabbit anti-KEAP1, Abclonal, A1820,1:200) overnight at 4 °C, followed by incubation with a secondary antibody kit (Proteintech, Cat No. PK10006) at room temperature for 1 h, and staining with DAB reagent. Finally, the sections were restained with hematoxylin, dehydrated through gradient alcohol, mounted, and photographed under a microscope (Olympus BX61, Shinjuku-ku, Japan).

Quantitative real-time PCR

Total RNA was extracted from cells with RNAex Pro RNA Reagent (AG, Changsha, China) and SteadyPure RNA Extraction Kit (AG) following manufacturer's instructions. Reverse transcription was performed with Evo M-MLV Premix for qPCR (AG) with 500 ng RNA. The target cDNA was amplified by SYBR Green Pro Taq HS qPCR Kit (AG) and Bio-Rad CFX96 for detection (Bio-Rad, CA, USA). Gene expression was analyzed using the $2^{-\Delta\Delta Ct}$ method with *ACTB* as a control. The primers are listed in Supplementary Table 1.

Western blot

Cells were lysed by RIPA lysis with 1% PMSF on ice for 30 min, and then centrifuged with 12,000×*g* at 4 °C for 30 min. The protein concentration was determined by an enhanced BCA protein assay kit (Beyotime). Equal amounts of protein were separated by an appropriate concentration of the SDS-PAGE gel and transferred into a polyvinylidene difluoride (PVDF) membrane with a Mini Trans-Blot Module (Bio-Rad). 5% skim milk was used to block the membrane for 1 h at room temperature. The membrane was incubated with different primary antibodies (rabbit anti-NRF2, Abclonal, A3577,1:1000; rabbit anti-NOTCH3, Abclonal, A13522,1:1000; rabbit anti-GCLC, Abclonal, A4499, 1:1000; mouse anti-NQO1, Proteintech, 67240-1-Ig,1:10000; rabbit anti-GPX2, Abclonal, A15999, 1:1000; rabbit anti-β-ACTIN, Bioworld, AP0060, 1:2000) at 4 °C overnight and incubated secondary antibodies (Goat-Anti-Mouse, ZENBIO,511103, 1:5000; Goat-Anti-Rabbit, ZENBIO,511203, 1:5000) sequentially for 1 h at room temperature. Target proteins were visualized using BeyoECL Plus kit (Beyotime).

3D sphere formation

Single cells (3000/well) were resuspended in the complete growth medium mixed with Matrigel (80% concentration), and then seeded in 24-well plates. The plates were incubated at 37 °C for 20 min to allow gelation. Upon completed gelation, 400 µl of completed growth medium was added in each well and cultured in a humidified incubator at 37°C with 5% CO_2. Medium was changed every 3 days. The spheres were photographed and the size was measured on day 14.

Cell apoptosis measurement

To measure cell apoptosis, resuspended cells were incubated with Annexin V-mCherry (Beyotime, Shanghai, China) for 15 min in the dark. Zombie Aqua (Biolegend, San Diego, USA) was used as a counterstain to discriminate necrotic/dead cells from apoptotic cells. Stained cells were analyzed in an ACEA NovoCyteTM flow cytometer. Data were analyzed with FlowJo software (Ashland, Oregon, USA).

Flow cytometric analysis

To perform cell surface marker staining, the cells were dissociated with 0.25% Trypsin-EDTA and stained with PE-conjugated anti-CD133 (Cat. #311104; BioLegend, San Diego, USA) or APC-conjugated anti-CD44 (Cat. #338808; BioLegend) antibodies in FACS buffer (1 X PBS, 2% FBS, 0.2 mM EDTA) for 30 min with live/dead staining dye (Zombie Aqua, Biolegend) to exclude dead cells (Supplementary Fig. 3). Stained cells were analyzed in an ACEA NovoCyteTM flow cytometer. Data were analyzed with FlowJo software (Ashland, Oregon, USA).

ALDEFLUOR assays

The cellular ALDH activities were measured with the ALDEFLUOR assay (STEMCELL Technologies, Vancouver, Canada). Cells were resuspended and incubated with 1 µM ALDEFLUOR and incubated at 37 °C with 5% CO_2 for 40 min. PI staining was used to exclude dead cells (Supplementary Fig. 6A). For negative controls, ALDH activity was blocked with 15 µM of the selective ALDH inhibitor DEAB. After incubation, cells were washed and underwent FACS analysis in an ACEA NovoCyteTM flow cytometer. ALDH activity was determined by the ALDEFLUOR signal (488 nm excitation, 515/20 nm emission). ALDH-positive cells were identified by fluorescence exceeding the region for control cells that were under identical conditions but with DEAB. Data were analyzed with FlowJo software (Ashland, Oregon, USA).

Reactive oxygen species analysis

The oxidation-sensitive fluorescent probe DCFH-DA(Beyotime) was used to detect the generation of ROS following the manufacturer's instructions. Briefly, Cells were digested and washed three times with HBSS without phenol red and then incubated with 10 μM DCF-DA for 30 min in the dark at 37 °C. Cells then were analyzed in an ACEA NovoCyteTM flow cytometer. Data were analyzed with FlowJo software (Ashland, Oregon, USA).

Statistical analysis

The data was analyzed using GraphPad Prism version 9.5 software and presented as mean ± SD, derived from experiments with a minimum of three replicates. Differences between 2 groups were analyzed by a 2-tailed Students' *t* test. A *P* value of 0.05 or less was considered statistically significant. Differences among 3 or more groups were analyzed using one-way ANOVA. The determination of sample size was informed by preliminary data, which provided insights into the variance within each group and the distinctions between them.

DATA AVAILABILITY

The RNA sequence fastq files will be uploaded to Genome Sequence Archive (GSA) in BIG Data Center (http://bigd.big.ac.cn/gsa), Chinese Academy of Sciences, with an accession number HRA008343.

REFERENCES

1. Johnson DE, Burtness B, Leemans CR, Lui VWY, Bauman JE, Grandis JR. Head and neck squamous cell carcinoma. Nat Rev Dis Prim. 2020;6:1–22.
2. Sung H, Ferlay J, Siegel RL, Laversanne M, Soerjomataram I, Jemal A, et al. Global Cancer Statistics 2020: GLOBOCAN estimates of incidence and mortality worldwide for 36 cancers in 185 countries. CA Cancer J Clin. 2021;71:209–49.
3. Li Q, Tie Y, Alu A, Ma X, Shi H. Targeted therapy for head and neck cancer: signaling pathways and clinical studies. Sig Transduct Target Ther. 2023;8:1–28.
4. Zhou G, Liu Z, Myers JN. TP53 mutations in head and neck squamous cell carcinoma and their impact on disease progression and treatment response. J Cell Biochem. 2016;117:2682–92.
5. Chung CH, Ely K, McGavran L, Varella-Garcia M, Parker J, Parker N, et al. Increased epidermal growth factor receptor gene copy number is associated with poor prognosis in head and neck squamous cell carcinomas. J Clin Oncol. 2006;24:4170–6.
6. Iglesias-Bartolome R, Martin D, Gutkind JS. Exploiting the head and neck cancer oncogenome: widespread PI3K-mTOR pathway alterations and novel molecular targets. Cancer Discov. 2013;3:722–5.
7. Leemans CR, Braakhuis BJM, Brakenhoff RH. The molecular biology of head and neck cancer. Nat Rev Cancer. 2011;11:9–22.
8. Furukawa M, Xiong Y. BTB protein Keap1 targets antioxidant transcription factor Nrf2 for ubiquitination by the Cullin 3-Roc1 ligase. Mol Cell Biol. 2005;25:162–71.
9. Kansanen E, Kuosmanen SM, Leinonen H, Levonen A-L. The Keap1-Nrf2 pathway: mechanisms of activation and dysregulation in cancer. Redox Biol. 2013;1:45–9.
10. Ramos-Gomez M, Kwak MK, Dolan PM, Itoh K, Yamamoto M, Talalay P, et al. Sensitivity to carcinogenesis is increased and chemoprotective efficacy of enzyme inducers is lost in nrf2 transcription factor-deficient mice. Proc Natl Acad Sci USA. 2001;98:3410–5.
11. Ramos-Gomez M, Dolan PM, Itoh K, Yamamoto M, Kensler TW. Interactive effects of nrf2 genotype and oltipraz on benzo[a]pyrene-DNA adducts and tumor yield in mice. Carcinogenesis. 2003;24:461–7.
12. Chio IIC, Jafarnejad SM, Ponz-Sarvise M, Park Y, Rivera K, Palm W, et al. NRF2 promotes tumor maintenance by modulating mrna translation in pancreatic cancer. Cell. 2016;166:963–76.
13. Lignitto L, LeBoeuf SE, Homer H, Jiang S, Askenazi M, Karakousi TR, et al. Nrf2 activation promotes lung cancer metastasis by inhibiting the degradation of Bach1. Cell. 2019;178:316–29.e18.
14. Fox DB, Garcia NMG, McKinney BJ, Lupo R, Noteware LC, Newcomb R, et al. NRF2 activation promotes the recurrence of dormant tumour cells through regulation of redox and nucleotide metabolism. Nat Metab. 2020;2:318–34.
15. Taniguchi S, Elhance A, Van Duzer A, Kumar S, Leitenberger JJ, Oshimori N. Tumor-initiating cells establish an IL-33–TGF-β niche signaling loop to promote cancer progression. Science. 2020;369:eaay1813.
16. Feng L, Zhao K, Sun L, Yin X, Zhang J, Liu C, et al. SLC7A11 regulated by NRF2 modulates esophageal squamous cell carcinoma radiosensitivity by inhibiting ferroptosis. J Transl Med. 2021;19:367.
17. Singh A, Daemen A, Nickles D, Jeon S-M, Foreman O, Sudini K, et al. NRF2 activation promotes aggressive lung cancer and associates with poor clinical outcomes. Clin Cancer Res. 2021;27:877–88.
18. Forstrom JW, Zakowski JJ, Tappel AL. Identification of the catalytic site of rat liver glutathione peroxidase as selenocysteine. Biochemistry. 1978;17:2639–44.
19. Schwarz M, Löser A, Cheng Q, Wichmann-Costaganna M, Schädel P, Werz O, et al. Side-by-side comparison of recombinant human glutathione peroxidases identifies overlapping substrate specificities for soluble hydroperoxides. Redox Biol. 2023;59:102593.
20. Esworthy RS, Doroshow JH, Chu F-F. The beginning of GPX2 and 30 years later. Free Radic Biol Med. 2022;188:419–33.
21. Lee E, Choi A, Jun Y, Kim N, Yook JI, Kim SY, et al. Glutathione peroxidase-1 regulates adhesion and metastasis of triple-negative breast cancer cells via FAK signaling. Redox Biol. 2020;29:101391.
22. Cheng L, He Q, Liu B, Chen L, Lv F, Li X, et al. SGK2 promotes prostate cancer metastasis by inhibiting ferroptosis via upregulating GPX4. Cell Death Dis. 2023;14:1–14.
23. Ren Z, Liang H, Galbo PM, Dharmaratne M, Kulkarni AS, Fard AT, et al. Redox signaling by glutathione peroxidase 2 links vascular modulation to metabolic plasticity of breast cancer. Proc Natl Acad Sci USA. 2022;119:e2107266119.
24. Ding Y, Chen X, Liu C, Ge W, Wang Q, Hao X, et al. Identification of a small molecule as inducer of ferroptosis and apoptosis through ubiquitination of GPX4 in triple negative breast cancer cells. J Hematol Oncol. 2021;14:19.
25. Peng D, Hu T, Soutto M, Belkhiri A, Zaika A, El-Rifai W. Glutathione peroxidase 7 has potential tumour suppressor functions that are silenced by location-specific methylation in oesophageal adenocarcinoma. Gut. 2014;63:540–51.
26. Nguyen TTM, Nguyen TH, Kim HS, Dao TTP, Moon Y, Seo M, et al. GPX8 regulates clear cell renal cell carcinoma tumorigenesis through promoting lipogenesis by NNMT. J Exp Clin Cancer Res. 2023;42:42.
27. Yang M, Zhu X, Shen Y, He Q, Qin Y, Shao Y, et al. GPX2 predicts recurrence-free survival and triggers the Wnt/β-catenin/EMT pathway in prostate cancer. PeerJ. 2022;10:e14263.
28. Lei Z, Tian D, Zhang C, Zhao S, Su M. Clinicopathological and prognostic significance of GPX2 protein expression in esophageal squamous cell carcinoma. BMC Cancer. 2016;16:410.
29. Ahmed KM, Veeramachaneni R, Deng D, Putluri N, Putluri V, Cardenas MF, et al. Glutathione peroxidase 2 is a metabolic driver of the tumor immune microenvironment and immune checkpoint inhibitor response. J Immunother Cancer. 2022;10:e004752.
30. Cancer Genome Atlas Network. Comprehensive genomic characterization of head and neck squamous cell carcinomas. Nature. 2015;517:576–82.
31. Torrente L, DeNicola GM. Targeting NRF2 and its downstream processes: opportunities and challenges. Annu Rev Pharm Toxicol. 2022;62:279–300.
32. Győrffy B. Integrated analysis of public datasets for the discovery and validation of survival-associated genes in solid tumors. Innovation. 2024;5:100625.
33. Kensler TW, Wakabayashi N, Biswal S. Cell survival responses to environmental stresses via the Keap1-Nrf2-ARE pathway. Annu Rev Pharmacol Toxicol. 2007;47:89–116.
34. Iida K, Itoh K, Kumagai Y, Oyasu R, Hattori K, Kawai K, et al. Nrf2 is essential for the chemopreventive efficacy of oltipraz against urinary bladder carcinogenesis. Cancer Res. 2004;64:6424–31.
35. Kim T-H, Hur E, Kang S-J, Kim J-A, Thapa D, Lee YM, et al. NRF2 blockade suppresses colon tumor angiogenesis by inhibiting hypoxia-induced activation of HIF-1α. Cancer Res. 2011;71:2260–75.
36. Pillai R, Hayashi M, Zavitsanou A-M, Papagiannakopoulos T. NRF2: KEAPing tumors protected. Cancer Discov. 2022;12:625–43.
37. Ge W, Zhao K, Wang X, Li H, Yu M, He M, et al. iASPP Is an antioxidative factor and drives cancer growth and drug resistance by competing with Nrf2 for Keap1 binding. Cancer Cell. 2017;32:561–73.e6.
38. Zhou Y, Chen Y, Shi Y, Wu L, Tan Y, Li T, et al. FAM117B promotes gastric cancer growth and drug resistance by targeting the KEAP1/NRF2 signaling pathway. J Clin Invest. 2023;133:e158705.
39. Tan W, Zhang K, Chen X, Yang L, Zhu S, Wei Y, et al. GPX2 is a potential therapeutic target to induce cell apoptosis in lenvatinib against hepatocellular carcinoma. J Adv Res. 2023;44:173–83.
40. Lu X, Liu R, Liao Y, Cui L, Sun H, Zhang D, et al. ACVRL1 drives resistance to multitarget tyrosine kinase inhibitors in colorectal cancer by promoting USP15-mediated GPX2 stabilization. BMC Med. 2023;21:366.
41. Dannenmann B, Lehle S, Hildebrand DG, Kübler A, Grondona P, Schmid V, et al. High glutathione and glutathione peroxidase-2 levels mediate cell-type-specific DNA damage protection in human induced pluripotent stem cells. Stem Cell Rep. 2015;4:886–98.
42. Ludwig N, Szczepanski MJ, Gluszko A, Szafarowski T, Azambuja JH, Dolg L, et al. CD44(+) tumor cells promote early angiogenesis in head and neck squamous cell carcinoma. Cancer Lett. 2019;467:85–95.
43. Xu X, Chai S, Wang P, Zhang C, Yang Y, Yang Y, et al. Aldehyde dehydrogenases and cancer stem cells. Cancer Lett. 2015;369:50–7.

44. Wang J-Q, Yang Y, Cai C-Y, Teng Q-X, Cui Q, Lin J, et al. Multidrug resistance proteins (MRPs): structure, function and the overcoming of cancer multidrug resistance. Drug Resist Updates. 2021;54:100743.
45. de Souza I, Monteiro LKS, Guedes CB, Silva MM, Andrade-Tomaz M, Contieri B, et al. High levels of NRF2 sensitize temozolomide-resistant glioblastoma cells to ferroptosis via ABCC1/MRP1 upregulation. Cell Death Dis. 2022;13:1–13.
46. Lu J, Ye X, Fan F, Xia L, Bhattacharya R, Bellister S, et al. Endothelial cells promote the colorectal cancer stem cell phenotype through a soluble form of Jagged-1. Cancer Cell. 2013;23:171–85.
47. Cui Y, Chen H, Xi R, Cui H, Zhao Y, Xu E, et al. Whole-genome sequencing of 508 patients identifies key molecular features associated with poor prognosis in esophageal squamous cell carcinoma. Cell Res. 2020;30:902–13.
48. Cancer Genome Atlas Research Network. Comprehensive genomic characterization of squamous cell lung cancers. Nature. 2012;489:519–25.
49. Chang D, Shain AH. The landscape of driver mutations in cutaneous squamous cell carcinoma. npj Genom Med. 2021;6:1–10.
50. Kerins MJ, Ooi A. A catalogue of somatic NRF2 gain-of-function mutations in cancer. Sci Rep. 2018;8:12846.
51. Hayes JD, Dinkova-Kostova AT. The Nrf2 regulatory network provides an interface between redox and intermediary metabolism. Trends Biochem Sci. 2014;39:199–218.
52. Panday S, Talreja R, Kavdia M. The role of glutathione and glutathione peroxidase in regulating cellular level of reactive oxygen and nitrogen species. Microvasc Res. 2020;131:104010.
53. Banning A, Deubel S, Kluth D, Zhou Z, Brigelius-Flohé R. The GI-GPx gene is a target for Nrf2. Mol Cell Biol. 2005;25:4914–23.
54. Cho H-Y, van Houten B, Wang X, Miller-DeGraff L, Fostel J, Gladwell W, et al. Targeted deletion of nrf2 impairs lung development and oxidant injury in neonatal mice. Antioxid Redox Signal. 2012;17:1066–82.
55. Xu H, Hu C, Wang Y, Shi Y, Yuan L, Xu J, et al. Glutathione peroxidase 2 knockdown suppresses gastric cancer progression and metastasis via regulation of kynurenine metabolism. Oncogene. 2023;42:1994–2006
56. Hall MD, Marshall TS, Kwit ADT, Miller Jenkins LM, Dulcey AE, Madigan JP, et al. Inhibition of glutathione peroxidase mediates the collateral sensitivity of multidrug-resistant cells to tiopronin. J Biol Chem. 2014;289:21473–89.
57. Yuan L, Li S, Chen Q, Xia T, Luo D, Li L, et al. EBV infection-induced GPX4 promotes chemoresistance and tumor progression in nasopharyngeal carcinoma. Cell Death Differ. 2022;29:1513–27.
58. Lee JW, Lee H, Chun YS, Ahn J, Moon JY, Kim DK, et al. Characterization of chemoresistant human non-small cell lung cancer cells by metabolic and lipidomic profiling. Metabolomics. 2023;19:80.
59. Ballatori N, Krance SM, Marchan R, Hammond CL. Plasma membrane glutathione transporters and their roles in cell physiology and pathophysiology. Mol Asp Med. 2009;30:13–28.
60. Huang T, Song X, Xu D, Tiek D, Goenka A, Wu B, et al. Stem cell programs in cancer initiation, progression, and therapy resistance. Theranostics. 2020;10:8721–43.
61. Manni W, Min W. Signaling pathways in the regulation of cancer stem cells and associated targeted therapy. MedComm (2020). 2022;3:e176.
62. Fendler A, Bauer D, Busch J, Jung K, Wulf-Goldenberg A, Kunz S, et al. Inhibiting WNT and NOTCH in renal cancer stem cells and the implications for human patients. Nat Commun. 2020;11:929.
63. Liu L, Tao T, Liu S, Yang X, Chen X, Liang J, et al. An RFC4/Notch1 signaling feedback loop promotes NSCLC metastasis and stemness. Nat Commun. 2021;12:2693.
64. Jackstadt R, van Hooff SR, Leach JD, Cortes-Lavaud X, Lohuis JO, Ridgway RA, et al. Epithelial NOTCH signaling rewires the tumor microenvironment of colorectal cancer to drive poor-prognosis subtypes and metastasis. Cancer Cell. 2019;36:319–36.e7.
65. Wang F, Zhang J, Tang H, Pang Y, Ke X, Peng W, et al. Nup54-induced CARM1 nuclear importation promotes gastric cancer cell proliferation and tumorigenesis through transcriptional activation and methylation of Notch2. Oncogene. 2022;41:246–59.
66. Zhang Y-Q, Liang Y-K, Wu Y, Chen M, Chen W-L, Li R-H, et al. Notch3 inhibits cell proliferation and tumorigenesis and predicts better prognosis in breast cancer through transactivating PTEN. Cell Death Dis. 2021;12:1–16.
67. Kondratyev M, Pesic A, Ketela T, Stickle N, Beswick C, Shalev Z, et al. Identification of acquired Notch3 dependency in metastatic Head and Neck Cancer. Commun Biol. 2023;6:538.
68. Okazaki K, Anzawa H, Liu Z, Ota N, Kitamura H, Onodera Y, et al. Enhancer remodeling promotes tumor-initiating activity in NRF2-activated non-small cell lung cancers. Nat Commun. 2020;11:5911.
69. Bialk P, Wang Y, Banas K, Kmiec EB. Functional gene knockout of NRF2 increases chemosensitivity of human lung cancer A549 cells in vitro and in a xenograft mouse model. Mol Ther Oncolytics. 2018;11:75–89.

AUTHOR CONTRIBUTIONS

JXY and JM conceived and supervised the study. JXY, LXY, ZC, and RJ contributed to data interpretation, manuscript writing, and performed experiments. QHX, LB, SWXR, LR, ZA, and LQL contributed to the data collection and analysis. All authors read and approved the final manuscript.

FUNDING

This study was supported by the National Key Research and Development Program of China (2021YFC2501800) and the National Natural Science Foundation of China (No. 32270863).

COMPETING INTERESTS

The authors declare no competing interests.

ETHICAL APPROVAL

Human HNSCC tissues were obtained from patients who received curative surgery at Jiangxi Cancer Hospital (Jiangxi, China). The research was conducted in accordance with the applicable national ethical standards. This study was approved by the Research Ethics Committee of Jiangxi Cancer Hospital (approval number: 2024ky008). Animal experiments were approved by the Institutional Animal Care and Use Committee of Zhejiang University (approval number: 20221576).

INFORMED CONSENT

Written informed consent was obtained from patients.

CONSENT FOR PUBLICATION

The authors declare their consent for this publication.

ADDITIONAL INFORMATION

Supplementary information The online version contains supplementary material available at https://doi.org/10.1038/s41389-024-00536-z.

Correspondence and requests for materials should be addressed to Ming Jiang.

Reprints and permission information is available at http://www.nature.com/reprints

Publisher's note Springer Nature remains neutral with regard to jurisdictional claims in published maps and institutional affiliations.